Dynamical resilience to disorder: the dilute Hubbard model on the Lieb lattice

L. Oliveira-Lima,[1] N. C. Costa,[2,3] J. Pimentel de Lima,[1] R. T. Scalettar,[4] and R. R. dos Santos[2]

[1] *Departamento de Física, Universidade Federal do Piauí, 64049-550 Teresina PI, Brazil*
[2] *Instituto de Física, Universidade Federal do Rio de Janeiro Cx.P. 68.528, 21941-972 Rio de Janeiro RJ, Brazil*
[3] *International School for Advanced Studies (SISSA), Via Bonomea 265, 34136, Trieste, Italy*
[4] *Department of Physics, University of California, Davis, CA 95616, USA*

(Dated: January 21, 2022)

In itinerant systems, electron-electron interactions may lead to the formation of local magnetic moments and their effective exchange coupling, which in turn gives rise to long-range magnetic order. Therefore, when moment formation is weakened, such as in the single-band Hubbard model on a square lattice with the on-site repulsion being randomly switched off on a fraction x of sites, magnetic order is suppressed beyond some critical x_c, which was found to lie below the classical percolation threshold, $x_c^{(\mathrm{perc,sq})}$. Here we study dilute magnetism in flat band systems, namely in the Hubbard model on a 'Lieb' lattice. Interestingly, we show that magnetic order persists to x almost twice as large as the classical percolation threshold for the lattice, thus emphasizing the central role of electron itinerancy to the magnetic response. The analysis of the orbital-resolved order parameters reveals that the contribution of the four-fold coordinated 'd' sites to magnetism is dramatically affected by dilution, while the localized 'p' states of the flat band provide the dominant contribution to long-range correlations. We also examine the transport properties, which suggest the existence of an insulator-to-metal transition in the same range of the critical magnetic dilution.

PACS numbers: 71.10.Fd, 02.70.Uu

arXiv:1912.04918v3 [cond-mat.str-el] 9 Apr 2020

I. INTRODUCTION

The study of magnetic systems with quenched random site or bond dilution has raised fundamental issues over the years. One question which was the subject of considerable scrutiny was whether or not critical exponents are altered; the Harris criterion suggests they remain at pure system values as long as the specific heat exponent $\alpha > 0$ [1]. Initial explorations focused on classical spin models. For instance, Monte Carlo simulations of the square lattice bond-diluted [2] and site-diluted [3] Ising models verified 'strong universality'. The exponents were found to be the same as that of the pure system (even though $\alpha = 0$). Another issue of special experimental interest relates to dilute magnetic semiconductors, since even a few of percent transition-metal atoms introduce ferromagnetism, which might be harnessed to change device functionality [4, 5]. The possibility of magnetic order even in the high dilution limit emphasizes the crucial role of coupling of moments through the free carriers, an effect not captured in Ising-like models of spins interacting purely through local exchange coupling.

Indeed, in dilute magnetic *insulators* where there is no long-range Rudermann-Kittel-Kasuya-Yosida (RKKY) [6–8] coupling and interactions are only between neighboring sites, geometrical aspects dominate the suppression of magnetic order as the interactions between the localized spins are randomly switched off. This can be achieved by either replacing atoms possessing localized moments by non-magnetic atoms (the site-dilution problem), or by removing atoms mediating the superexchange interaction between localized spins (the bond-dilution problem) [9, 10]. In both cases, the underlying lattice structure is fundamental, since only in the percolating regime in which at least one path of connected sites spans the whole lattice [11] can long-range magnetic order be established. The ground state magnetization decreases steadily and vanishes at some critical concentration of sites (s) or bonds (b), such that $x_c^{(\mathrm{s})} \leq x_c^{(\mathrm{b})}$ [11], beyond which no long-range order can be sustained [9, 10].

For itinerant systems, however, the situation is quite different. Consider the repulsive Hubbard model in which the on-site interaction U is switched off on a fraction x of sites. Ulmke et al. [12] considered a square lattice at half-filling and ratio of on-site interaction to hopping integral $U/t = 8$. Long range antiferromagnetic (AF) order disappears at $x_c \gtrsim 0.43 \pm 0.07$. The large uncertainty results from the challenges in doing the finite size and zero temperature extrapolations. Nevertheless, this strong coupling critical value is consistent with the classical site-percolation threshold, $x_c^{(\mathrm{perc,sq})} = 0.41$ [11]. On the other hand, at weaker coupling $U/t = 4$, deviations from classical percolation have been found [13–16]. For the square lattice x_c is significantly less than the expected percolation value [14, 16] [17].

The fact that, at coupling $U/t = 4$, the dilution threshold for itinerant electrons is lower than the classical, geometry-dependent, percolation value suggests that enhanced double occupancy plays a role in weakening magnetic order before the percolation threshold is reached. Interestingly, the recovery of the percolation value at $U/t \sim 8$ is consistent with the fact that this is the crossover interaction strength to the regime where the Hubbard model is well described by the Heisenberg Hamiltonian [18–20]. That is, charge fluctuations are strongly suppressed and no longer play

a role on the effects of dilution in the eventual magnetic response.

In this paper we extend this understanding of dilution in itinerant electron system to the Hubbard model on the Lieb lattice [21–29], also known as a decorated square lattice, or as the 'CuO$_2$ lattice'; see Fig. 1 (a). This geometry is realized in the CuO$_2$ sheets of high-T_c cuprates [30] and also has been emulated in photonic and optical lattices [31–37], as well as in atomic manipulation of electronic states in Cu(111) surfaces [38]. The Lieb lattice geometry allows us to explore diluted itinerant electron systems in an entirely new physical context, one in which a flat band is present at half-filling (for the noninteracting case), as displayed in Fig. 1 (c), and for which compact localized states are present even for strong hopping disorder [39]. As a consequence of these features, the electron dynamics on the Lieb lattice is quite different from that on more conventional structures, leading to the possibility of alternate magnetic response when electron-electron interactions are taken into account. Indeed, the fact that the two sublattices have unequal numbers of sites already gives rise to unique physics even in the absence of dilution: a *ferrimagnetic* state at half-filling [40, 41], with a large contribution of the p-band to this long-range ordered state [25]. Here we investigate the robustness of this ferrimagnetic state in presence of site disorder. However, from the outset we stress that due to limitations on the system sizes used for quantum systems [42–44], in particular to the itinerant electronic case, numerical calculations can rarely provide critical exponents with sufficient accuracy to settle issues related to the Harris criterion. So, although we have discussed this issue to lend broad perspective to our work, we will not attempt to address this issue directly.

The layout of the paper is as follows. In Sec. II we present details of the model, the calculational procedure, determinant Quantum Monte Carlo (DQMC), and the magnetic and transport observables used to characterize the system. The results are presented and discussed in Sec. III, while Sec. IV summarizes our findings.

II. MODEL AND METHODOLOGY

The Hubbard Hamiltonian for the Lieb lattice reads

$$\begin{aligned}\widehat{\mathcal{H}} = &- t_{pd}\sum_{\mathbf{r}\sigma}\left(d^\dagger_{\mathbf{r}\sigma}p^x_{\mathbf{r}\sigma} + d^\dagger_{\mathbf{r}\sigma}p^y_{\mathbf{r}\sigma} + \text{H.c}\right)\\ &- t_{pd}\sum_{\mathbf{r}\sigma}\left(d^\dagger_{\mathbf{r}\sigma}p^x_{\mathbf{r}+\hat{x}\sigma} + d^\dagger_{\mathbf{r}\sigma}p^y_{\mathbf{r}+\hat{y}\sigma} + \text{H.c}\right)\\ &+ \sum_{\mathbf{r},\alpha}U^\alpha_{\mathbf{r}}\left(n^\alpha_{\mathbf{r}\uparrow} - \frac{1}{2}\right)\left(n^\alpha_{\mathbf{r}\downarrow} - \frac{1}{2}\right)\\ &+ \sum_{\mathbf{r},\sigma,\alpha}(\varepsilon_\alpha - \mu)n^\alpha_{\mathbf{r}\sigma}\ , \end{aligned} \tag{1}$$

with $d_{\mathbf{r}\sigma}$, $p^x_{\mathbf{r}\sigma}$, and $p^y_{\mathbf{r}\sigma}$ being standard annihilation electron operators in second-quantized formalism, while

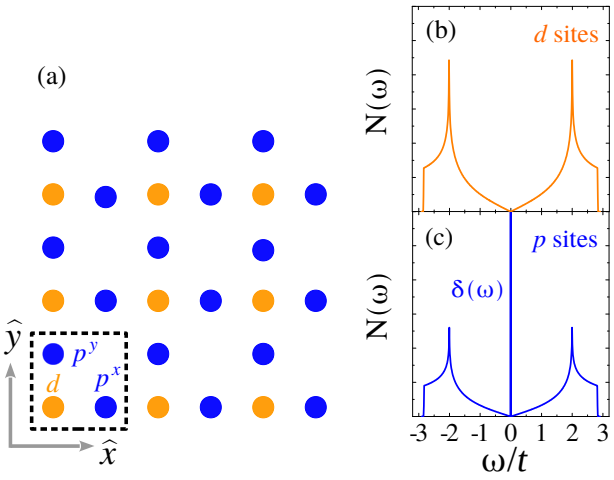


FIG. 1. (Color online) (a) The Lieb (or CuO$_2$) lattice. The fourfold coordinated d sites appear in lighter color (orange) and belong to one sublattice, while the twofold coordinated p sites appear in darker color (blue) and belong to the other sublattice. The dashed box corresponds to the unit cell. Panels (b) and (c) respectively show the non-interacting density of states on d and p sites.

$n^\alpha_{\mathbf{r}\sigma}$ are the number operators for their corresponding orbitals, $\alpha = d$, p^x, or p^y; our notation therefore follows closely that of the CuO$_2$ lattice realization. The first two terms on the right hand side of Eq. (1) denote the inter- and intra-cell hopping between d- and p-orbitals, respectively, while the third term corresponds to a site and orbital-dependent local repulsive interaction. The last term involves the onsite energies ε_α and the chemical potential μ, which we set to $\varepsilon_\alpha = \mu = 0$, a choice which makes each orbital precisely half-filled. The hopping integral is taken as $t_{pd} = 1$, thus defining the energy scale.

We model dilution by allowing for random distributions of $U^\alpha_{\mathbf{r}}$, such that a fraction x of the sites have their interaction strength suppressed,

$$U^\alpha_{\mathbf{r}} = \begin{cases} U & \text{with probability } (1-x);\\ 0 & \text{with probability } x. \end{cases} \tag{2}$$

The $U = 0$ sites no longer support moment formation as a result of charge fluctuations. Our simulations focus on the intermediate coupling value $U/t_{pd} = 4$, since this is the case where previous work has found that magnetic order vanishes (below) away from the percolation value. It is important to notice that, for the noninteracting case, since the bandwidth of the Lieb lattice is $W_{\text{lieb}}/t = 4\sqrt{2}$ [see, e.g., Fig. 1 (b)-(c)], being smaller than the one for the square lattice ($W_{\text{sqr}}/t = 8$), we effectively have a larger U/W for the former. Therefore, one should naively expect stronger geometrical effects for this choice of interaction strength.

We investigate the ground state properties of the Hamiltonian (1) by means of DQMC simulations [45–49]. This is an unbiased numerical method

based on an auxiliary-field decomposition of the interaction which maps onto free fermions moving in a fluctuating space and (imaginary) time dependent potential. The first key step is a separation (the Trotter-Suzuki decoupling) of the noncommuting parts of the Hamiltonian: $\widehat{\mathcal{H}}_0$ containing the terms quadratic in the fermion creation and destruction operators and the quartic term $\widehat{\mathcal{H}}_{\rm U}$ which occur in the partition function $\mathcal{Z} = {\rm Tr}\, e^{-\beta\widehat{\mathcal{H}}} = {\rm Tr}\,[(e^{-\Delta\tau(\widehat{\mathcal{H}}_0+\widehat{\mathcal{H}}_{\rm U})})^M] \approx {\rm Tr}\,[e^{-\Delta\tau\widehat{\mathcal{H}}_0}e^{-\Delta\tau\widehat{\mathcal{H}}_{\rm U}}e^{-\Delta\tau\widehat{\mathcal{H}}_0}e^{-\Delta\tau\widehat{\mathcal{H}}_{\rm U}}\dots]$, where $\beta = M\Delta\tau$, with $\Delta\tau$ being the grid of the imaginary-time coordinate axis. This decomposition leads to an error proportional to $(\Delta\tau)^2$, which can be systematically reduced as $\Delta\tau \to 0$. Here, we choose $\Delta\tau = 0.125$, which is small enough so that the systematic errors for the magnetic structure factor are comparable to the statistical ones (from the Monte Carlo sampling). The second central step is a discrete Hubbard-Stratonovich (HS) transform [46] on the two-particle terms $e^{-\Delta\tau\widehat{\mathcal{H}}_{\rm U}}$ which converts them also to quadratic in the fermion operators. In this way the resulting trace of fermions propagating in an auxiliary bosonic field, whose components depend on the space and imaginary-time lattice coordinates, can be performed.

The HS fields are sampled by standard Monte Carlo techniques, allowing the measurement of Green's functions, and other physical quantities including spin, charge, and pair correlation functions. The DQMC method, as with many fermionic QMC approaches, in general suffers from the minus-sign problem when particle-hole symmetry (PHS) is broken [50]. Here, however, we stress that the Lieb lattice is bipartite and the introduction of randomness in the interaction strength preserves PHS at half-filling, so that the sign problem is absent for this case. A detailed introduction to DQMC can be found, e.g. in Refs. 49, 51, and 52.

The magnetic response of the system is probed by the real space spin-spin correlation functions

$$c_{\alpha\gamma}(\boldsymbol{\ell}) = \frac{1}{3}\langle \mathbf{S}^{\alpha}_{\mathbf{r}_0} \cdot \mathbf{S}^{\gamma}_{\mathbf{r}_0+\boldsymbol{\ell}} \rangle\,, \tag{3}$$

with $\mathbf{r}_0$ being the position of a given unit cell, while α and γ denote the orbitals (d, p^x, or p^y). The Fourier transform of $c_{\alpha\gamma}(\boldsymbol{\ell})$ is the magnetic structure factor,

$$S(\mathbf{q}) = \frac{1}{N_s}\sum_{\alpha,\gamma}\sum_{\boldsymbol{\ell}} c_{\alpha\gamma}(\boldsymbol{\ell}) e^{i\mathbf{q}\cdot\boldsymbol{\ell}}\,, \tag{4}$$

where the number of sites is $N_s = 3L^2$, with L being the linear size of the underlying Bravais square lattice. $S(\mathbf{q})$ peaks at the dominant magnetic wavevector of the system. The existence of a global *ferro*magnetically ordered state is probed by the usual Huse finite-size scaling form [53] with $\mathbf{q} = (0,0)$,

$$\frac{S(0,0)}{L^2} = (m^F)^2 + \frac{A}{L}, \tag{5}$$

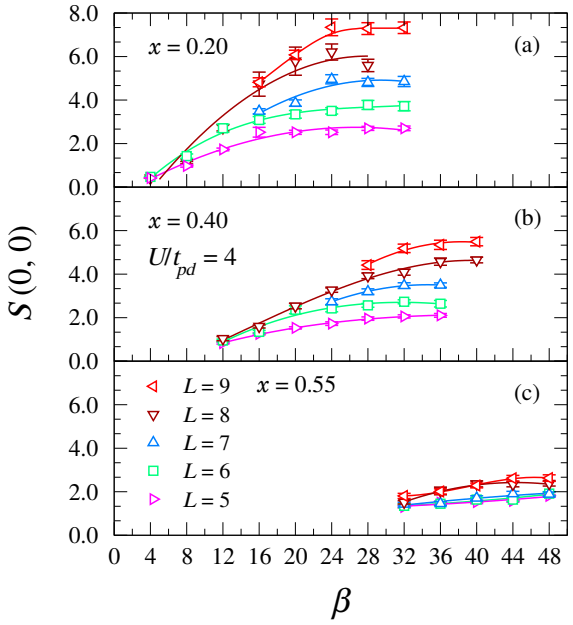


FIG. 2. (Color online) The global FM spin structure factor as a function of inverse of temperature for (a) $x = 0.20$, (b) $x = 0.40$, (c) $x = 0.55$, and different lattice sizes L. Solid lines are guides to the eye. Here, and in all subsequent figures, when not shown, error bars are smaller than the symbol size.

where m^F is the associated order parameter, and A is a constant.

In addition, for a global ferromagnetic arrangement, Eq. (4) allows us to separate the individual orbital contributions as

$$S(0,0) = \big(S_{d\,d} + S_{p^x\,p^x} + S_{p^y\,p^y} + 2S_{p^x\,p^y} + 2S_{d\,p^x} + 2S_{d\,p^y}\big)/3\,, \tag{6}$$

with

$$S_{\alpha\gamma} = \frac{1}{L^2}\sum_{\boldsymbol{\ell}} c_{\alpha\gamma}(\boldsymbol{\ell})\,, \tag{7}$$

where we use the fact that $S_{\alpha\gamma} = S_{\gamma\alpha}$. Since the $\pi/2$ real space rotational invariance is recovered after disorder averaging, one should find $S_{p^x\,p^x} = S_{p^y\,p^y} \approx S_{p^x\,p^y}$, and $S_{d\,p^x} = S_{d\,p^y}$. It is therefore useful to define

$$S_{p\,p} = \frac{1}{4}\big[S_{p^x\,p^x} + S_{p^y\,p^y} + 2S_{p^x\,p^y}\big]\,, \tag{8}$$

and

$$S_{d\,p} = \frac{1}{2}\big[S_{d\,p^x} + S_{d\,p^y}\big]\,, \tag{9}$$

which leads to

$$S(0,0) = \frac{1}{3}\big[S_{d\,d} + 4S_{p\,p} - 4|S_{d\,p}|\big]\,. \tag{10}$$

The last term in Eq. (10) enters in absolute value because the d-p spin correlations are always antiferromagnetic at

half-filling, i.e. $S_{dp} < 0$ (in accordance to rigorous results derived in Ref. 54), and indicative of the *ferri*magnetic nature which combines a nonzero overall ferromagnetism with anti-alignment of d and p spins within the unit cell.

The individual components of the structure factors obey the same finite size scaling form[53], allowing us to extract the orbital-resolved order parameters in the thermodynamic limit,

$$(m^F_{dd})^2 = \frac{S_{dd}}{L^2} + \frac{a}{L}, \tag{11}$$

$$(m^F_{pp})^2 = \frac{S_{pp}}{L^2} + \frac{b}{L}, \tag{12}$$

$$(m^{AF}_{dp})^2 = \frac{|S_{dp}|}{L^2} + \frac{c}{L}, \tag{13}$$

where a, b and c are constants.

Finally, the metallic or insulating character of the system is probed with two independent quantities. One is the direct-current conductivity,

$$\sigma_{dc} = \frac{\beta^2}{\pi}\Lambda_{xx}(\mathbf{q}=\mathbf{0}, \tau=\beta/2), \tag{14}$$

where

$$\Lambda_{xx}(\mathbf{q},\tau) = \langle j_x(\mathbf{q},\tau) j_x(-\mathbf{q},0)\rangle, \tag{15}$$

with $j_x(\mathbf{q},\tau)$ being the Fourier transform of

$$j_x(\mathbf{i},\tau) = \mathrm{e}^{\tau\mathcal{H}}\left[it\sum_{\sigma}\left(c^{\dagger}_{\mathbf{i}+\mathbf{x}\sigma}c_{\mathbf{i}\sigma} - c^{\dagger}_{\mathbf{i}\sigma}c_{\mathbf{i}+\mathbf{x}\sigma}\right)\right]\mathrm{e}^{-\tau\mathcal{H}}; \tag{16}$$

This approximation has been extensively used to identify metal-insulator transitions [55, 56]. The other quantity is the electronic compressibility, defined as

$$\kappa = \frac{1}{n^2}\frac{\partial n}{\partial \mu}, \tag{17}$$

where n is the global electronic density. We should note that in principle our data for κ could suffer from the sign-problem when the chemical potential moves slightly around half-filling in the finite difference implementation of Eq. (17). However, in a regime where κ is small, the sign problem is less serious, because even though a non-zero chemical potential is applied, the density stays close to half-filling. Indeed, we have systematically checked that the average sign was always close to 1 within the range of parameters analyzed. Therefore, our data for the compressibility are free from the minus-sign problem.

III. RESULTS

We consider lattices with linear sizes up to $L = 9$ ($N_s \leq 243$), and we take $U/t_{pd} = 4$ throughout the paper. Further, in what follows our results are obtained by averaging over 20-60 disorder realizations, depending on the temperature and lattice sizes; this procedure keeps the error bars in the correlation functions small enough to give rise to unambiguous extrapolations. The disorder configurations are generated in a canonical ensemble, i.e. for a given concentration, x, of free sites one randomly chooses xN_s sites to set $U = 0$, so that there are no fluctuations in the number of free sites. For dilution fractions x which do not correspond to an integer number of sites for a given L, we perform a weighted average over the adjacent integers.

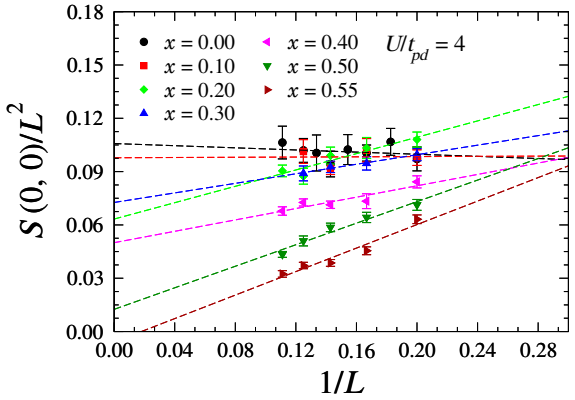


FIG. 3. (Color online) Finite-size scaling of the normalized global ground state structure factor for different impurity concentrations.

Figure 2 illustrates the behavior of the global uniform structure factor $S(0,0)$ with the inverse temperature, $\beta = 1/T$, for three different concentrations of free sites. In each case $S(0,0)$ approaches an asymptotic value for sufficiently large β, reflecting the fact that, in an ordered phase, the correlation length is limited by the finite size of the lattice. These large β values give $S(0,0)$ at $T = 0$ (for the given system size and concentration) and are used for the scaling analysis of Eq. (5). The outcome is depicted in Fig. 3. For each concentration the ground state magnetization in the thermodynamic limit is obtained from the intercept with the vertical axis ($1/L = 0$). These, in turn, are plotted as a function of the concentration in Fig. 4.

From Fig. 4 we see that the global magnetization decreases steadily with increasing disorder and vanishes around $x_c \approx 0.55$, a value more than twice as large as the classical site-percolation threshold for the Lieb lattice, $x_c^{(\mathrm{perc,Lieb})} \approx 0.26$ [57, 58]. This clearly shows that the disorder-induced transition is not purely geometric.

In order to understand why the magnetic behavior on the diluted Lieb lattice is more robust, in the sense that $x_c > x_c^{(\mathrm{perc,Lieb})}$, we must examine the orbital-resolved order parameters. Figure 5 shows their temperature dependence for a given linear system size. We see that the dominant correlations between electrons on p orbitals are ferromagnetic, and so are those on d sites; by contrast, when one electron is on a p-site and the other on a d-site, the correlations are antiferromagnetic, justifying the

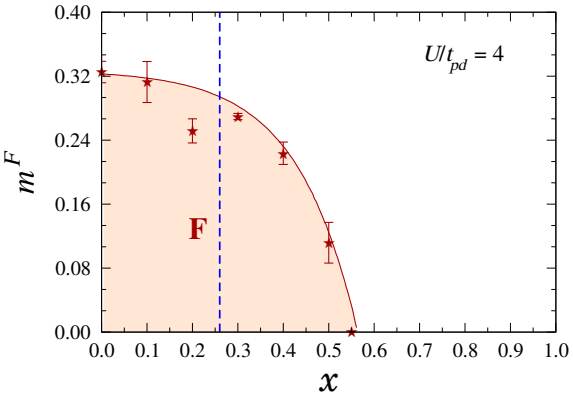


FIG. 4. (Color online) Global ground state ferromagnetic order parameter m^F as a function of dilution fraction, x. The error bars are due to the uncertainties in the $1/L \to 0$ extrapolation; see Fig. 3. The solid curve is a guide to the eye for the magnetization, while the vertical dashed line marks the classical site-percolation threshold for the Lieb lattice.

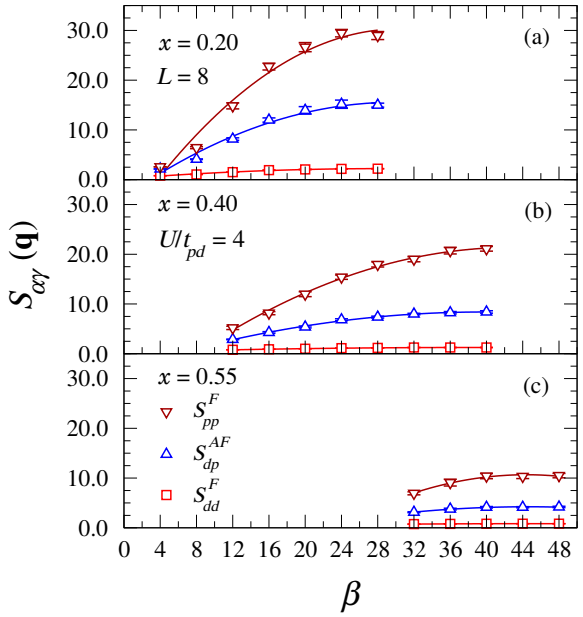


FIG. 5. (Color online) Orbitally-resolved contributions to the structure factor from d-d (squares), d-p (triangles), and p-p (inverted triangles) correlations as functions of the inverse temperature, for fixed $L = 8$ and (a) $x = 0.20$, (b) $x = 0.40$, and (c) $x = 0.55$. Solid lines are guides to the eye.

form of Eq. 10. Following the procedure adopted for the global structure factor, in Fig. 6 we extrapolate the low temperature results to $L \to \infty$. The thermodymanic limit intercepts with the vertical axis are plotted in Fig. 7.

A strong coupling analysis for the clean system [25] attributes the robustness of the pp FM order parameter to the p spins locking into triplets. In contrast, the weakness of the dd correlations originates in a shielding by these surrounding triplets. This picture in fact persists to seemingly rather small values of U/t_{pd}, as a result of the flatness of p-band, which makes the ratio of the interaction to bandwidth large. The formation of such triplets seems to be only weakly affected if $U = 0$ on all d-sites: as discussed in Ref. 25, magnetic order persists even in this limiting case. Upon random dilution, one should notice that the long-range behavior of d-sites (m^F_{dd}) is strongly suppressed for a small dilution strength, while magnetism is dominated by the p-sublattice, as shown in Fig. 7: the pp contribution to the magnetization is much stronger than those involving d-sites, both in intensity and in its resilience to disorder, sustaining order well beyond the classical percolation threshold. It is worth noticing that the robustness of the long-range behavior of p-sites is due to their coupling to d-sites, which may restore the triplets even when $U = 0$ on a given p-site. As displayed in Fig. 7, long-range antiferromagnetic correlations between p and d-electrons (i.e., m^{AF}_{dp}) occur even for $m^F_{dd} = 0$, and has almost the same threshold as m^F_{pp}. It therefore emphasizes the importance of d-electrons to global magnetism, and seems to be the key feature for the occurence of magnetism beyond the classical percolation limit.

Once the disorder threshold is exceeded, there are not enough strongly repulsive U-sites to sustain an insulating state at half-filling, and we expect a metallic state to set in. This can be checked with the aid of the conductivity, calculated through Eq. (14). Figure 8 (a) shows the

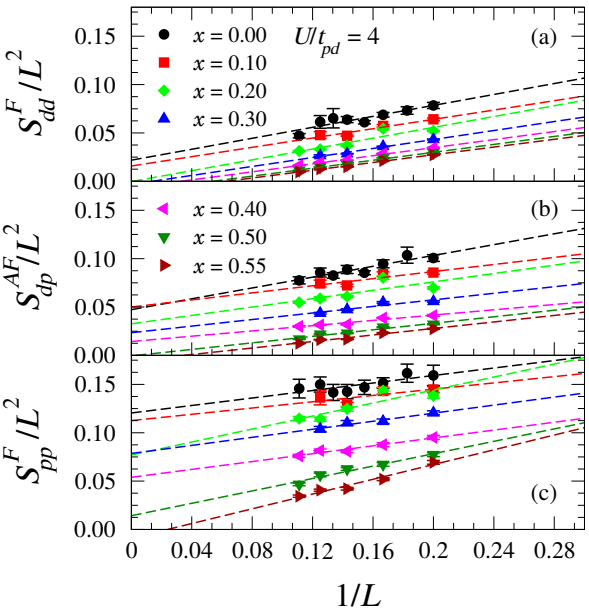


FIG. 6. (Color online) Finite-size scaling of the normalized, orbitally-resolved structure factors of (a) d-d, (b) d-p, and (c) p-p contributions for different dilutions.

temperature dependence of σ_{dc} for different disorder concentrations, while Figure 8 (b) shows σ_{dc} as a function of concentration, for different temperatures. Two distinct regimes are clearly identified: insulating, when $\sigma_{\rm dc}$ decreases as the temperature decreases, and metallic, when $\sigma_{\rm dc}$ increases as the temperature decreases. One

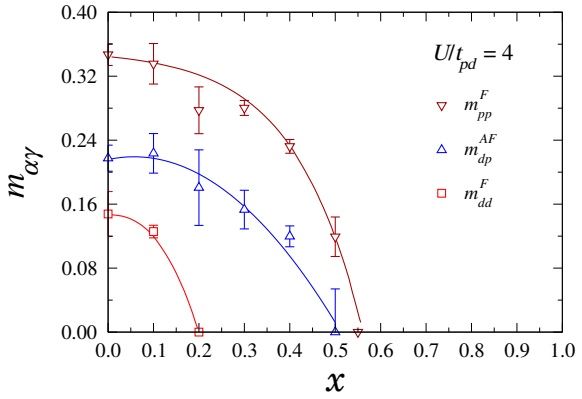


FIG. 7. (Color online) Extrapolated ($L \to \infty$) values of the orbitally-resolved contributions to the order parameter, obtained from the scaling of their structure factors; see Fig. 6. Solid lines are guides to the eye.

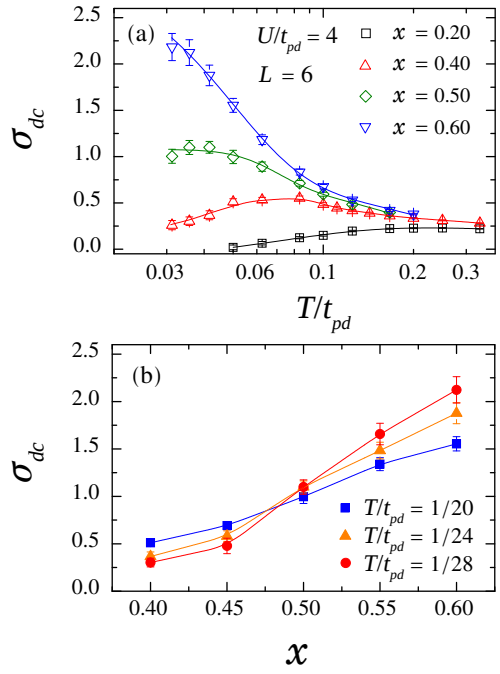


FIG. 8. (Color online) Conductivity (a) as a function of temperature, for different dilutions, and (b) as a function of dilution, for different temperatures. The solid lines are guides to the eye. Both presentations of the data suggest insulating behavior for $x < x_c \sim 0.5$ and metallic behavior for $x > x_c \sim 0.5$.

can roughly estimate that the change in behavior occurs at $x_c^{(\sigma_{dc})} = 0.50 \pm 0.03$, which is consistent with the results suggesting a change in magnetic behavior at the same x_c. The transition across x_c is therefore from an insulating ferrimagnetic phase to a metallic paramagnetic one.

Further evidence in favor of the insulator-metal transition is provided by the compressibility, Eq. (17). Figure 9 shows the *global* compressibility, the change in the *overall* density with chemical potential. We see that

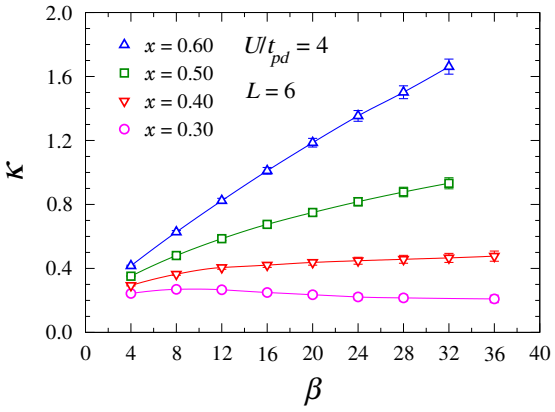


FIG. 9. (Color online) Global compressibility as a function of the inverse temperature, for different dilution concentrations, x. The solid lines are guides to the eye.

for $x = 0.3$ and 0.4 the system has a small, temperature independent value of κ, while for $x = 0.5$ and 0.6, κ increases with β. In Figure 10 the compressibility is broken into individual contributions from p and d sites, and we see that the dominant behavior comes from p sites, which are the ones forming the flat band. That is, x_c defines a value above which the p sites become weakly compressible. It is also worth noticing that for $x > x_c$, κ_p seems to diverge at low temperatures, a behavior already present in the noninteracting case due to the dispersionless middle band [see, e.g., Fig. 1 (c)]. Thus, for $x > x_c$, the transport properties resemble those for the noninteracting one, despite the presence of electron-electron interactions on a subset of sites.

The following picture emerges from the combination of data for the magnetic structure factor, conductivity, and compressibility: The low temperature insulating ferrimagnetic state can accommodate extra electrons on the $U = 0$ sites at low energetic cost, provided there are not too many of them. As dilution increases, more $U = 0$ p sites become available, and the system becomes fully compressible. One should also notice that, since there is an energetic cost to break the triplets formed by spins on p sites, the compressibility is reduced as the temperature decreases, for $x \lesssim 0.30$, and grows faster for $x \gtrsim 0.40$.

IV. CONCLUSIONS

Studies of the Periodic Anderson Model [59–61] and of the single band Hubbard model with random dilution of the on-site interaction [12–16] have provided opportunities for the exploration of magnetic order in systems possessing both sites where moments form and those for which charge fluctuations are allowed. By considering dilution on the repulsive Hubbard model on a Lieb lattice, in which the on-site repulsion U is switched off on a fraction x of sites, we have established some new features of this problem.

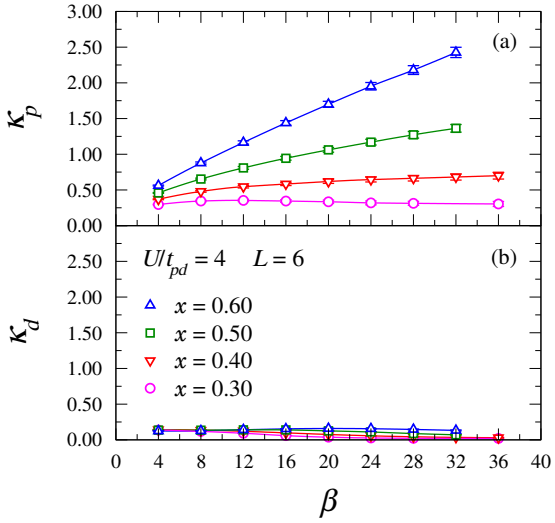


FIG. 10. (Color online) Site-resolved compressibility as a function of the inverse temperature, for different dilution concentrations, x: (a) compressibility on p sites, and (b) compressibility on d sites. Solid lines are guides to the eye.

In particular, although studies of the diluted square lattice Hubbard model suggested the critical concentration for $U = 0$ sites is *less than* the percolation value, we have shown here that on the Lieb lattice magnetic order is *more robust* than one might expect from percolation arguments: the percolation threshold, x_c, is higher than the one solely determined by the geometry of the lattice, $x_c^{(\mathrm{perc,Lieb})}$. While a dynamic (i.e. interaction-driven) influence on x_c had already been noted [14, 16] for the attractive Hubbard model at half-filling (which has a corresponding behavior in the repulsive case), there the classical percolation threshold provides an *upper* bound to the quantum case. A second observation is that, simultaneously with the 'percolative' magnetic transition, the system undergoes an insulator to metal transition, as evidenced by both the dc-conductivity and the compressibility. These properties are a direct consequence of the flat p-band displayed by the non-interacting Lieb lattice. Our results therefore show that disordered quantum itinerant systems display a non-trivial interplay between dynamics and lattice geometry leading to features with no counterpart in classical systems.

Previous works [12–16] have suggested that the presence of two regimes, one at strong coupling where $x_c \sim x_c^{(\mathrm{perc,sq})}$, and one at weaker coupling where $x_c < x_c^{(\mathrm{perc,sq})}$, might be connected to the two distinct physical pictures for the origin of antiferromagnetism (AF) in the half-filled single-band square lattice Hubbard model. For large U/t one thinks of a Mott insulating state in which a superexchange interaction $J = 4t^2/U$ couples neighboring spins. A (quantum) Heisenberg spin description is appropriate in this regime. On the other hand, at weak coupling, AF can be viewed as arising from a spin-density wave instability driven by Fermi surface nesting. In this case, the $U = 0$ band structure and electron itinerancy play a central role. Our work suggests that, although a criterion for x_c based purely on the strength of U/t might be correct for a single band model, a more complex picture is necessary to understand the multiple band case. Specifically, the orbitally-resolved magnetic order parameters $m_{\alpha\gamma}$ must be analyzed, and might vanish at very different dilution fractions. Finally, it would also be interesting to verify whether the metal-insulator and the ferrimagnetic transitions always take place concomitantly, or may occur at different regions of the parameter space, e.g. if turns out that $x_c^{\mathrm{Fer}} \neq x_c^{\mathrm{Ins}}$, one could have a ferrimagnetic metal or a nonmagnetic Mott insulating state. Further work is needed to clarify this interesting issue.

ACKNOWLEDGMENTS

The work of RTS was supported by the grant DESC0014671 funded by the U.S. Department of Energy, Office of Science. Financial support from the Brazilian Agencies CAPES, CNPq, FAPERJ and FAPEPI is also gratefully acknowledged. The authors are grateful to T. Paiva and S.L.A. de Queiroz for discussions. N.C.C. acknowledges PRACE for awarding him access to Marconi at CINECA, Italy.

[1] A. B. Harris, "Effect of random defects on the critical behaviour of Ising models," Journal of Physics C: Solid State Physics **7**, 1671–1692 (1974).
[2] D. Zobin, "Critical behavior of the bond-dilute two-dimensional Ising model," Phys. Rev. B **18**, 2387–2390 (1978).
[3] P. H. L. Martins and J. A. Plascak, "Universality class of the two-dimensional site-diluted Ising model," Phys. Rev. E **76**, 012102 (2007).
[4] S. A. Wolf, D. D. Awschalom, R. A. Buhrman, J. M. Daughton, S. von Molnár, M. L. Roukes, A. Y. Chtchelkanova, and D. M. Treger, "Spintronics: A spin-based electronics vision for the future," Science **294**, 1488–1495 (2001).
[5] Igor Žutić, Jaroslav Fabian, and S. Das Sarma, "Spintronics: Fundamentals and applications," Rev. Mod. Phys. **76**, 323–410 (2004).
[6] M. A. Ruderman and C. Kittel, "Indirect exchange coupling of nuclear magnetic moments by conduction electrons," Phys. Rev. **96**, 99–102 (1954).
[7] Tadao Kasuya, "A theory of metallic ferro- and antiferromagnetism on Zener's model," Progress of Theoretical Physics **16**, 45–57 (1956).

[8] Kei Yosida, "Magnetic properties of Cu-Mn alloys," Phys. Rev. **106**, 893–898 (1957).

[9] R. B. Stinchcombe, "Dilute magnetism," in *Phase Transitions and Critical Phenomena*, Vol. 7, edited by C. Domb and J. L. Lebowitz (Academic, New York, 1983) pp. 152–280.

[10] D. P. Belanger, "Experimental characterization of the Ising model in disordered antiferromagnets," Braz. J. Phys. **30**, 682–692 (2000).

[11] D. Stauffer and A. Aharony, *Introduction To Percolation Theory* (Taylor & Francis, 1994).

[12] M. Ulmke, P. J. H. Denteneer, R. T. Scalettar, and G. T. Zimanyi, "Enhancement of long-range antiferromagnetic order by nonmagnetic impurities in the Hubbard model," Europhys. Lett. **42**, 655 (1998).

[13] G. Litak and B. L. Györffy, "Random negative-U Hubbard model," Phys. Rev. B **62**, 6629–6637 (2000).

[14] Daniel Hurt, Evan Odabashian, Warren E. Pickett, Richard T. Scalettar, Felipe Mondaini, Thereza Paiva, and Raimundo R. dos Santos, "Destruction of superconductivity by impurities in the attractive Hubbard model," Phys. Rev. B **72**, 144513 (2005).

[15] Saurabh Pradhan and G. Venketeswara Pai, "Effect of site dilution in the two-dimensional attractive Hubbard model," Phys. Rev. B **98**, 165142 (2018).

[16] Felipe Mondaini, Thereza Paiva, Raimundo R. dos Santos, and R. T. Scalettar, "Disordered two-dimensional superconductors: Roles of temperature and interaction strength," Phys. Rev. B **78**, 174519 (2008).

[17] These Quantum Monte Carlo studies were actually done on superconductivity and charge order in the attractive Hubbard model, but the conclusions for magnetism in the repulsive case can be obtained through a particle-hole transformation [62, 63].

[18] R. Staudt, M. Dzierzawa, and A. Muramatsu, "Phase diagram of the three-dimensional Hubbard model at half filling," Eur. Phys. J. B **17**, 411–415 (2000).

[19] E. Kozik, E. Burovski, V. W. Scarola, and M. Troyer, "Néel temperature and thermodynamics of the half-filled three-dimensional Hubbard model by diagrammatic determinant Monte Carlo," Phys. Rev. B **87**, 205102 (2013).

[20] Ehsan Khatami, "Three-dimensional Hubbard model in the thermodynamic limit," Phys. Rev. B **94**, 125114 (2016).

[21] Kazuto Noda, Akihisa Koga, Norio Kawakami, and Thomas Pruschke, "Ferromagnetism of cold fermions loaded into a decorated square lattice," Phys. Rev. A **80**, 063622 (2009).

[22] C. Weeks and M. Franz, "Topological insulators on the Lieb and perovskite lattices," Phys. Rev. B **82**, 085310 (2010).

[23] An Zhao and Shun-Qing Shen, "Quantum anomalous hall effect in a flat band ferromagnet," Phys. Rev. B **85**, 085209 (2012).

[24] M. Niţă, B. Ostahie, and A. Aldea, "Spectral and transport properties of the two-dimensional Lieb lattice," Phys. Rev. B **87**, 125428 (2013).

[25] Natanael C. Costa, Tiago Mendes-Santos, Thereza Paiva, Raimundo R. dos Santos, and Richard T. Scalettar, "Ferromagnetism beyond Lieb's theorem," Phys. Rev. B **94**, 155107 (2016).

[26] Martin Bercx, Johannes S. Hofmann, Fakher F. Assaad, and Thomas C. Lang, "Spontaneous particle-hole symmetry breaking of correlated fermions on the Lieb lattice," Phys. Rev. B **95**, 035108 (2017).

[27] Pramod Kumar, Tuomas I. Vanhala, and Päivi Törmä, "Temperature and doping induced instabilities of the repulsive Hubbard model on the Lieb lattice," Phys. Rev. B **96**, 245127 (2017).

[28] Joo-Hyeok Jeong, Hyunjoon Park, Dongkyu Kim, and Dong-Hee Kim, "Magnetic shell structure of 2D-trapped Fermi gases in the flat-band Lieb lattices," Applied Sciences **9** (2019), 10.3390/app9030365.

[29] P.T.T. Le and Mohsen Yarmohammadi, "Impurity-tuning of phase transition and mid-state in 2D spin Lieb lattice," Physica E: Low-dimensional Systems and Nanostructures **105**, 56 – 61 (2019).

[30] In this situation U_d on the copper orbitals is quite a bit larger than U_p on the oxygen orbitals.

[31] R. Shen, L. B. Shao, Baigeng Wang, and D. Y. Xing, "Single Dirac cone with a flat band touching on line-centered-square optical lattices," Phys. Rev. B **81**, 041410 (2010).

[32] D Guzmán-Silva, C Mejía-Cortés, M A Bandres, M C Rechtsman, S Weimann, S Nolte, M Segev, A Szameit, and R A Vicencio, "Experimental observation of bulk and edge transport in photonic Lieb lattices," New Journal of Physics **16**, 063061 (2014).

[33] Sebabrata Mukherjee, Alexander Spracklen, Debaditya Choudhury, Nathan Goldman, Patrik Öhberg, Erika Andersson, and Robert R. Thomson, "Observation of a localized flat-band state in a photonic Lieb lattice," Phys. Rev. Lett. **114**, 245504 (2015).

[34] Rodrigo A. Vicencio, Camilo Cantillano, Luis Morales-Inostroza, Bastián Real, Cristian Mejía-Cortés, Steffen Weimann, Alexander Szameit, and Mario I. Molina, "Observation of localized states in Lieb photonic lattices," Phys. Rev. Lett. **114**, 245503 (2015).

[35] Shintaro Taie, Hideki Ozawa, Tomohiro Ichinose, Takuei Nishio, Shuta Nakajima, and Yoshiro Takahashi, "Coherent driving and freezing of bosonic matter wave in an optical Lieb lattice," Science Advances **1** (2015), 10.1126/sciadv.1500854.

[36] Shiqiang Xia, Yi Hu, Daohong Song, Yuanyuan Zong, Liqin Tang, and Zhigang Chen, "Demonstration of flat-band image transmission in optically induced Lieb photonic lattices," Opt. Lett. **41**, 1435–1438 (2016).

[37] Falko Diebel, Daniel Leykam, Sebastian Kroesen, Cornelia Denz, and Anton S. Desyatnikov, "Conical diffraction and composite Lieb bosons in photonic lattices," Phys. Rev. Lett. **116**, 183902 (2016).

[38] M. R. Slot, T. S. Gardenier, P. H. Jacobse, C. P. van Miert, S. N. Kempkes, S. J. M. Zevenhuizen, C. Morais Smith, D. Vanmaekelbergh, and I Swart, "Experimental realization and characterization of an electronic Lieb lattice," Nat. Phys. **13**, 672–677 (2017).

[39] Ajith Ramachandran, Alexei Andreanov, and Sergej Flach, "Chiral flat bands: Existence, engineering, and stability," Phys. Rev. B **96**, 161104 (2017).

[40] Elliott H. Lieb, "Two theorems on the Hubbard model," Phys. Rev. Lett. **62**, 1201–1204 (1989).

[41] Elliott H. Lieb, "Two theorems on the Hubbard model," Phys. Rev. Lett. **62**, 1927–1927 (1989).

[42] Anders W. Sandvik, "Multicritical point in a diluted bilayer Heisenberg quantum antiferromagnet," Phys. Rev. Lett. **89**, 177201 (2002).

[43] Rastko Sknepnek, Thomas Vojta, and Matthias Vojta, "Exotic versus conventional scaling and universality in a disordered bilayer quantum Heisenberg antiferromagnet," Phys. Rev. Lett. **93**, 097201 (2004).

[44] Jhao-Hong Peng, L. W. Huang, D. R. Tan, and F. J. Jiang, "Validity of Harris criterion for two-dimensional quantum spin systems with quenched disorder," arXiv:1910.12705 (2019).

[45] R. Blankenbecler, D. J. Scalapino, and R. L. Sugar, "Monte Carlo calculations of coupled boson-fermion systems. I," Phys. Rev. D **24**, 2278–2286 (1981).

[46] J. E. Hirsch, "Discrete Hubbard-Stratonovich transformation for fermion lattice models," Phys. Rev. B **28**, 4059 (1983).

[47] J. E. Hirsch, "Two-dimensional Hubbard model: Numerical simulation study," Phys. Rev. B **31**, 4403–4419 (1985).

[48] S. R. White, D. J. Scalapino, R. L. Sugar, E. Y. Loh, J. E. Gubernatis, and R. T. Scalettar, "Numerical study of the two-dimensional Hubbard model," Phys. Rev. B **40**, 506–516 (1989).

[49] Raimundo R. dos Santos, "Introduction to quantum Monte Carlo simulations for fermionic systems," Braz. J. Phys. **33**, 36 – 54 (2003).

[50] Matthias Troyer and Uwe-Jens Wiese, "Computational complexity and fundamental limitations to fermionic quantum Monte Carlo simulations," Phys. Rev. Lett. **94**, 170201 (2005).

[51] F. Assaad, "Quantum Monte Carlo methods on lattices: The determinantal approach," in *Quantum Simulations of Complex Many-Body Systems: From Theory to Algorithms*, Vol. 10, edited by J Grotendorst, D. Marx, and A. Muramatsu (NIC Series,Jülich, Germany, 2002) pp. 99–156.

[52] J. Gubernatis, N. Kawashima, and P. Werner, *Quantum Monte Carlo Methods: Algorithms for Lattice Models* (Cambridge University Press, Cambridge, England, 2016).

[53] David A. Huse, "Ground-state staggered magnetization of two-dimensional quantum Heisenberg antiferromagnets," Phys. Rev. B **37**, 2380–2382 (1988).

[54] Shun-Qing Shen, Zhao-Ming Qiu, and Guang-Shan Tian, "Ferrimagnetic long-range order of the Hubbard model," Phys. Rev. Lett. **72**, 1280–1282 (1994).

[55] Nandini Trivedi, Richard T. Scalettar, and Mohit Randeria, "Superconductor-insulator transition in a disordered electronic system," Phys. Rev. B **54**, R3756–R3759 (1996).

[56] Rubem Mondaini, K. Bouadim, Thereza Paiva, and Raimundo R. dos Santos, "Finite-size effects in transport data from quantum Monte Carlo simulations," Phys. Rev. B **85**, 125127 (2012).

[57] Yuriy Yu. Tarasevich and Steven C. Van der Marck, "An investigation of site-bond percolation on many lattices," International Journal of Modern Physics C **10**, 1193–1204 (1999), arXiv:cond-mat/9906078.

[58] W. S. Oliveira, N. C. Costa, J. Pimentel de Lima, and Raimundo R. dos Santos, "Classical and quantum percolation on the Lieb lattice," (2019), unpublished.

[59] F. F. Assaad, "Depleted Kondo lattices: Quantum Monte Carlo and mean-field calculations," Phys. Rev. B **65**, 115104 (2002).

[60] N. C. Costa, M. V. Araújo, J. P. Lima, T. Paiva, R. R. dos Santos, and R. T. Scalettar, "Compressible ferrimagnetism in the depleted periodic Anderson model," Phys. Rev. B **97**, 085123 (2018).

[61] Lufeng Zhang, Tianxing Ma, Natanael C. Costa, Raimundo R. dos Santos, and Richard T. Scalettar, "Determinant quantum Monte Carlo study of exhaustion in the periodic Anderson model," Phys. Rev. B **99**, 195147 (2019).

[62] S. Robaszkiewicz, R. Micnas, and K. A. Chao, "Thermodynamic properties of the extended Hubbard model with strong intra-atomic attraction and an arbitrary electron density," Phys. Rev. B **23**, 1447–1458 (1981).

[63] Raimundo R. dos Santos, "Attractive Hubbard model on a triangular lattice," Phys. Rev. B **48**, 3976–3982 (1993).